Faraday Rotation Measurements in High-Energy-Density Plasmas Using Shaped Laser Beams

P.-A. Gourdain, A. Bachmann, I. N. Erez, F. Garrett, J. Hraki, S. McGaffigan, I. West-Abdallah, and J. R. Young

***Abstract*— Magnetic fields play an important role in plasma dynamics, yet it is a quantity difficult to measure accurately with physical probes, whose presence disturbs the very field they measure. The Faraday rotation (FR) of a polarized beam of light provides a mechanism to measure the magnetic field without disturbing the dynamics and has been used with great success in astrophysics and high-energy-density plasma science, where physical probes cannot be used. However, the rotation is typically small, which degrades the accuracy of the measurement. Since polarization cannot be measured directly, detectors rely on a polarizer to measure a small change in beam intensity instead. In this work, we show how beam shaping can improve FR measurements using an optical derivative setup. Since the rotation measurement is now strictly proportional to the beam shape and intensity, the system allows to improve the measurement accuracy simply by increasing the laser beam power.**

***Index Terms*— Plasma measurements.**

I. Introduction

FARADAY rotation (FR) [1], the change of light polarization caused by a magneto-ionized gas, thereafter called a plasma, has found applications in a wide range of disciplines over the years, from laser engineering [2] to astrophysics [3]. The landmark experiment, done by Michael Faraday in 1845 [4], showed that the polarization of an electromagnetic wave can be affected by a magnetic field parallel to the direction of propagation. The magnetic field triggers a birefringence inside the material, which, in turn, changes the polarization angle θ_{FR} as

$$\theta_{\mathrm{FR}} = V B L$$

where B is the magnetic field strength, projected along the direction of propagation of the electromagnetic wave, L is the propagation length in the birefringent medium, and V is the Verdet constant. A similar effect caused by magnetic fields transverse to the direction of propagation is called the Cotton–Mouton effect. While the Verdet constant can be difficult to compute for materials, it is relatively straightforward for a plasma [5]

$$\theta_{\mathrm{FR}}(x, y) = \frac{e^3 \lambda^2}{8\pi^2 \epsilon_0 m_e^2 c^3} \int_L n_e(x, y, z) \mathbf{B}(x, y, z) \cdot d\mathbf{z} \quad (1)$$

where e is the fundamental charge, λ is the laser wavelength, ϵ_0 is the vacuum permittivity, m_e is the electron mass, and n_e is the plasma electron number density. We supposed here that the light travels along the z-axis of our coordinate system, the x-axis being horizontal and the y-axis vertical. This dependence allows us to compute the magnetic field B_z, provided that the electron density n_e is already known. This effect has been used intensively to measure the magnetic field strength of the interstellar medium [6] by using background polarized sources, generating synchrotron radiations across a variety of wavelengths in the radio range [7]. FR was also used actively to highlight how bipolar jets spawned from accretion disks [8] are sensitive to the Hall effect [9], an effect [10] also found in high-energy-density plasma jets produced in the laboratory [11], [12]. Recently, the use of FR to measure magnetic fields in laboratory plasmas has become much more common in both low- [13], [14] and high-energy-density plasmas [15], [16], [17].

However, using FR to measure magnetic fields in the laboratory has proved challenging when using a visible laser [15] rather than microwaves [18] since (1) is a function of λ^2. For instance, if we used common parameters of laboratory astrophysics experiments done on MA-class machine [19], we get rotations on the order of 10 mrad for electron densities on the order of 10^{19} cm^{-3} and magnetic fields on the order of 100 mT, when using a green laser. The laser wavelength is a scaling factor in front of the integral of (1). As the wavelength becomes smaller, the cut-off density becomes

Received 7 September 2024; revised 12 November 2024; accepted 13 December 2024. Date of publication 30 December 2024; date of current version 28 January 2025. This work was supported in part by NSF CAREER under Grant PHY-1943939 and in part by the Laboratory for Laser Energetics Horton Fellowships. The review of this article was arranged by Senior Editor S. J. Gitomer. *(Corresponding author: P.-A. Gourdain.)*

P.-A. Gourdain, I. N. Erez, J. Hraki, and J. R. Young are with the Department of Physics and Astronomy and the Laboratory for Laser Energetics, University of Rochester, Rochester, NY 14627 USA (e-mail: gourdain@pas.rochester.edu).

A. Bachmann is with the Physics and Astronomy Department, UCLA, Los Angeles, CA 90095 USA.

F. Garrett is with the Department of Physics and Astronomy, University of Rochester, Rochester, NY 14627 USA.

S. McGaffigan is with the Physics Department, Columbia University, New York, NY 10027 USA.

I. West-Abdallah is with the Mechanical Engineering Department and the Laboratory for Laser Energetics, University of Rochester, Rochester, NY 14627 USA.

Color versions of one or more figures in this article are available at https://doi.org/10.1109/TPS.2024.3519036.

Digital Object Identifier 10.1109/TPS.2024.3519036

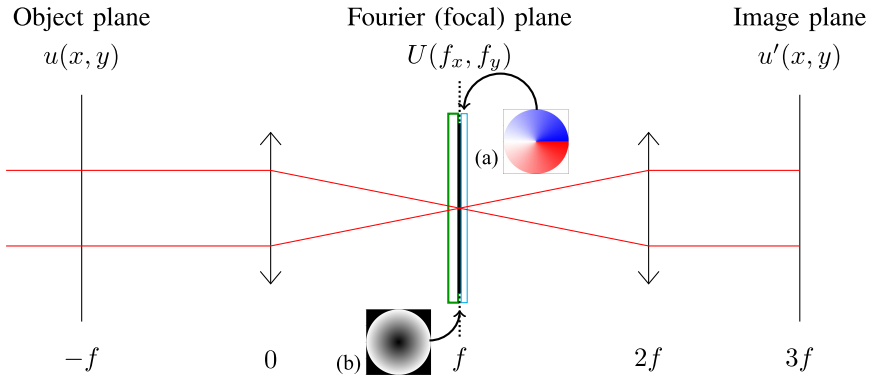

Fig. 1. Two-f system uses two identical lenses of focal length f. (a) S-waveplate is cyan and its effective polarizing angle, where red is $-\pi$ and blue is $+\pi$. (b) Neutral density filter with spatial distribution. The location of the filter is on the focal plane and its plate holder is shown in green. Both plates are drawn thicker for clarity. In reality, the thickness of the plates will be much smaller than f.

larger and deeper regions of the plasma can be probed [15]. However, the FR angle is now greatly reduced and becomes difficult to measure. In practice, this scaling factor acts as an attenuation factor.

In this article, we show that an S-waveplate combined with a neutral density filter with a radial variation scan be used to amplify the FR signal. In general, the S-waveplate [20] utilizes polarization to convert a linearly polarized Gaussian beam into a radially or azimuthally polarized beam [21]. It is complementary to the vortex plate [22], [23], [24], which affects the phase of the light rather than its polarization. The vortex plate achieves this by using a helical cavity with increasing depth corresponding to the azimuthal angle of the plate, changing the incoming phase of light azimuthally from 0 to 2 $m\pi$, where m is the plate charge. In contrast, the S-waveplate uses nanogratings with their alignment rotating with the plate's azimuthal angle to change the incoming polarization azimuthally from 0 to 2 $m\pi$, also using m as the plate charge. The proposed system gives the spatial derivative of the FR rotation signal, *de facto* removing the bias light from the probe beam. With the bias gone, the laser intensity can be increased, improving the signal-to-noise ratio of the measurement.

II. Optical Derivative of a Polarized Beam

When a light beam travels through the experimental setup shown in Fig. 1, its spatial constituents transform into its spectral (i.e., spatial frequency) constituents at the focal plane of the initial lens. This procedure finds mathematical expression through the utilization of the Fourier transform

$$U(f_x, f_y) = \int_{-\infty}^{+\infty}\int_{-\infty}^{+\infty} u(x, y)e^{-i2\pi x f_x}e^{-i2\pi y f_y}dxdy$$

where $U(f_x, f_y)$ is the intensity representing the Fourier transform of the light on the focal plane of the lens [25].

A. Description of the S-Waveplate Using Jones Matrix

The description of the S-waveplate can be effectively realized through the application of Jones matrices [26], [27]. This element can be divided into a retarder introducing a phase delay of $\varphi = \pi$ and a rotation matrix that imparts a rotation determined by the orientation ϕ of the nanogratings. Mathematically, the explicit expression for $\mathscr{S}$ takes the form

$$\mathscr{S} = e^{\frac{-i\varphi}{2}}\begin{bmatrix} \cos^2\phi + e^{i\varphi}\sin^2\phi & (1-e^{i\varphi})\cos\phi\sin\phi \\ (1-e^{i\varphi})\cos\phi\sin\phi & e^{i\varphi}\cos^2\phi + \sin^2\phi \end{bmatrix}$$

which can be simplified to

$$\mathscr{S}(x, y) = -i\begin{bmatrix} \cos\Theta(x, y) & \sin\Theta(x, y) \\ \sin\Theta(x, y) & -\cos\Theta(x, y) \end{bmatrix}. \quad (2)$$

Here, the local polarizing angle $\Theta(x, y)$ is twice the nanograting angle $\phi(x, y)$.

B. Beam With Variable Intensity and Constant Linear Polarization

We start with a linearly polarized laser beam having a constant polarization angle θ relative to the polarization of the S-plate. Any electric field with a stable polarization in the object plane can be expanded into a discrete summation of sine and cosine functions using the discrete Fourier transform as

$$\mathbf{E}(x, y) = \frac{\mathbf{A}_0}{2} + \sum_{n=1}^{+\infty}\cos(\mathbf{k}_n \cdot \mathbf{r})\mathbf{A}_n + \sin(\mathbf{k}_n \cdot \mathbf{r})\mathbf{B}_n \quad (3)$$

where $\mathbf{k}_n \cdot \mathbf{r} = k_{x,n}x + k_{y,n}y$, $\mathbf{A}_n = A_n\cos\theta\,\mathbf{x} + A_n\sin\theta\,\mathbf{y}$, and $\mathbf{B}_n = B_n\cos\theta\,\mathbf{x} + B_n\sin\theta\,\mathbf{y}$. Note that A_n and B_n can be complex. To illustrate the operation done in the Fourier plane by the S-waveplate, we examine each component of $\mathbf{E}(x, y)$ individually. We denote the component of $\mathbf{E}$ corresponding to $\mathbf{k} \in \{\mathbf{k}_1, \ldots, \mathbf{k}_n, \ldots, +\infty\}$ as $\mathbf{E}_\mathbf{k}(x, y) = \mathbf{A}_\mathbf{k}\cos(k_x x + k_y y) + \mathbf{B}_\mathbf{k}\sin(k_x x + k_y y)$. The Fourier transform of $\mathbf{E}_\mathbf{k}$ is given by

$$\begin{aligned}\mathscr{E}_\mathbf{k}(f_x, f_y) &= \left[\pi\delta\left(\frac{k_x}{2\pi} - f_x\right)\delta\left(\frac{k_y}{2\pi} - f_y\right) + \pi\delta\left(\frac{k_x}{2\pi} + f_x\right)\right. \\ &\quad \left.\times\,\delta\left(\frac{k_y}{2\pi} + f_y\right)\right]\mathbf{A}_\mathbf{k} \\ &\quad + \frac{1}{i}\left[\pi\delta\left(\frac{k_x}{2\pi} - f_x\right)\delta\left(\frac{k_y}{2\pi} - f_y\right) - \pi\delta\left(\frac{k_x}{2\pi} + f_x\right)\right. \\ &\quad \left.\times\,\delta\left(\frac{k_y}{2\pi} + f_y\right)\right]\mathbf{B}_\mathbf{k}.\end{aligned}$$

When introducing an S-waveplate at the Fourier plane (f_x, f_y) where the orientation of the local polarizing angle Θ varies azimuthally from 0 to 2π, the Jones matrix $\mathscr{S}$ of (2) can be expressed in term of the frequencies f_x and f_y as

$$\mathscr{S}(f_x, f_y) = -i\begin{bmatrix} \dfrac{f_x}{\sqrt{f_x^2+f_y^2}} & \dfrac{f_y}{\sqrt{f_x^2+f_y^2}} \\ \dfrac{f_y}{\sqrt{f_x^2+f_y^2}} & -\dfrac{f_x}{\sqrt{f_x^2+f_y^2}} \end{bmatrix}.$$

Now, we combine the S-waveplate with a neutral density filter whose transmission varies linearly with the radius ρ and is defined as [28]

$$\rho(f_x, f_y) = \sqrt{f_x^2+f_y^2}. \tag{4}$$

In practice, the transmission cannot exceed 1. While a scaling factor could be used, it is omitted here. The S-waveplate and the neutral density filter collectively constitute a new element denoted as $\mathscr{T}$, with a Jones matrix given by

$$\mathscr{T}(f_x, f_y) = -i\begin{bmatrix} f_x & f_y \\ f_y & -f_x \end{bmatrix}.$$

Upon performing the inverse Fourier transform of $\mathscr{E}_{\mathbf{k}}\mathscr{T}$, we obtain on the image plane [28]

$$\mathbf{E}'_{\mathbf{k}}(x, y) = -\mathscr{R}(-\theta)\nabla[A_{\mathbf{k}}\cos(\mathbf{k}\cdot\mathbf{r}) + B_{\mathbf{k}}\sin(\mathbf{k}\cdot\mathbf{r})] \tag{5}$$

where ∇ is the gradient operator and

$$\mathscr{R}(\theta) = \begin{bmatrix} \cos\theta & -\sin\theta \\ \sin\theta & \cos\theta \end{bmatrix} \tag{6}$$

is the 2-D rotation matrix for an angle θ. Since the main results of the article focus on intensities, we will drop the minus sign in (5) from later equations. As a result, the total electric field on the image plane is given by

$$\mathbf{E}'(x, y) = \nabla_{-\theta}E(x, y) \tag{7}$$

where the electric field $E(x, y)$ is the electric field along the polarization direction θ, that is,

$$E(x, y) = \frac{A_0}{2} + \sum_{n=1}^{+\infty} A_n\cos(\mathbf{k}_n\cdot\mathbf{r}) + B_n\sin(\mathbf{k}_n\cdot\mathbf{r})$$

and ∇_θ is the rotated gradient operator given by

$$\nabla_\theta = \mathscr{R}(\theta)\nabla \text{ or } \nabla_\theta = \begin{bmatrix} \cos\theta\,\partial_x - \sin\theta\,\partial_y \\ \sin\theta\,\partial_x + \cos\theta\,\partial_y \end{bmatrix}.$$

The resulting electric field of (7) is the gradient of the initial electric field along the polarization direction θ. However, its polarization is along the $-\theta$-direction now. Note that for a beam with a polarization angle $\theta = 0$ (polarization along the x-axis), ∇_θ becomes the usual gradient operator ∇. In this case, the S-waveplate/neutral density filter gives the gradient along two perpendicular polarization axes, allowing to measure $\partial_x E$ and $\partial_y E$ independently. This is a departure from the vortex plate setup [28] where the derivative along x and y were combined together.

C. Beam With Variable Intensity and Polarization

We again start with a linearly polarized laser beam with constant initial polarization angle θ_i with respect to the S-waveplate polarization. However, the electric field $E(x, y)$ has now acquired a variable polarization $\theta_{\text{FR}}(x, y)$ from a magnetoactive medium. We are dropping the coordinates x and y hereafter for the terms on the RHS of most equations. After exiting the medium, the electric field is given by

$$\mathbf{E}(x, y) = E\begin{bmatrix} \cos\theta \\ \sin\theta \end{bmatrix} \tag{8}$$

where $\theta = \theta_i + \theta_{\text{FR}}$. Since a spatial change in polarization simply corresponds to a change in intensity of the x- and y-polarization components of the beam, we can use (7) for each polarization independently to find the electric field at the exit of the augmented two-f system

$$\mathbf{E}'(x, y) = \nabla_0(E\cos\theta) + \nabla_{-\pi/2}(E\sin\theta)$$

which we can write explicitly as

$$\mathbf{E}'(x, y) = \begin{bmatrix} \partial_x(E\cos\theta) + \partial_y(E\sin\theta) \\ \partial_y(E\cos\theta) - \partial_x(E\sin\theta) \end{bmatrix}. \tag{9}$$

If θ is constant, then (9) is simply (7).

III. Implementation of an FR Measurement

A. Standard FR Measurement

It is typical to start with a y-polarized (i.e., vertically polarized) beam. The beam then passes through the magnetoactive medium, impinging an FR θ_{FR} to the polarization (see Fig. 2). At this point, a polarizer at $\pi/4$ from the vertical direction yields a new electric field

$$E_{\pi/4}(x, y) = E\cos(\alpha) \tag{10}$$

where $\alpha = \pi/4 - \theta_{\text{FR}}$ and $E(x, y)$ is the electric field strength. Now (10) can be turned into

$$E_{\pi/4}(x, y) = \frac{1}{\sqrt{2}}E[\cos(\theta_{\text{FR}}) + \sin(\theta_{\text{FR}})]. \tag{11}$$

The intensity can be written as

$$I_{\pi/4}(x, y) = \frac{1}{2}E^2[\cos(\theta_{\text{FR}}) + \sin(\theta_{\text{FR}})]^2. \tag{12}$$

As $\theta_{\text{FR}} \ll 1$ in most low-density magnetoactive media such as plasmas, we can do a Taylor expansion of (12) up to the first-order leading to

$$I_{\pi/4}(x, y) \simeq \frac{1}{2}E^2(1 + 2\theta_{\text{FR}}). \tag{13}$$

While this approach increases the measurement sensitivity compared to using a cross-polarizer downstream of the magnetoactive medium, the bias light [represented by the factor 1 in (13)] really reduces the signal-to-noise ratio.

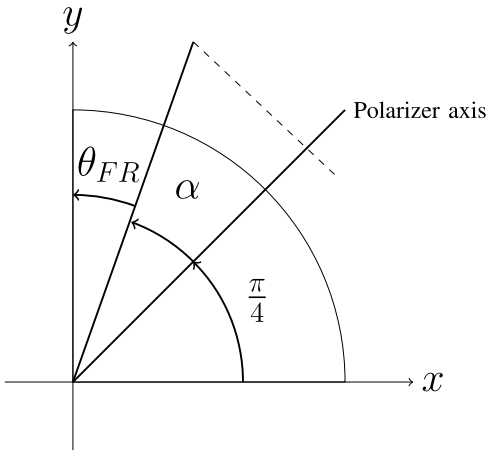

Fig. 2. Typical example of an FR measurement yielding an intensity that is proportional to $(1+\theta_{\mathrm{FR}})$ using a polarizer that is rotated by $\pi/4$ compared to the initial laser beam polarization.

B. FR Measurement With Homogeneous Beams

We look first at the case where the laser intensity is homogeneous, that is, $E(x,y) \simeq E_0$. We can choose $\theta_i = 0$. In this case, the electric field of (9) has a component along the x given by

$$E'_x(x,y) = E_0\big(\partial_x \cos\theta_{\mathrm{FR}} + \partial_y \sin\theta_{\mathrm{FR}}\big) \tag{14}$$

for the x-polarization and

$$E'_y(x,y) = E_0\big(\partial_y \cos\theta_{\mathrm{FR}} - \partial_x \sin\theta_{\mathrm{FR}}\big) \tag{15}$$

for the y-polarization. Since $\theta_{\mathrm{FR}} \ll 1$ the zeroth order of (14) is

$$E'_x(x,y) \simeq E_0 \partial_y \theta_{\mathrm{FR}}. \tag{16}$$

In this case, the zeroth order of the intensity of the x-polarization is

$$I'_x(x,y) \simeq |E_0|^2 \partial_y \theta^2_{\mathrm{FR}}. \tag{17}$$

Following the same line of thinking, (15) gives

$$E'_y(x,y) \simeq -E_0 \partial_x \theta_{\mathrm{FR}} \tag{18}$$

with an intensity

$$I'_y(x,y) \simeq |E_0|^2 \partial_x \theta^2_{\mathrm{FR}}. \tag{19}$$

We clearly see that the sensitivity of the measurement is reduced compared to (13) as we are looking at the square of the FR angle derivative. However, while the FR signal is still proportional to E^2 in (17) and (19), the bias signal of (13) has now disappeared. So, the sensitivity can be recovered simply by increasing the power of the input laser.

C. FR Measurement Using Beam Shaping

Most high-power laser beams can have some degree of controlled heterogeneity [29]. In this case, (9) yields

$$\mathbf{E}'(x,y) = E\begin{bmatrix} \cos\theta\partial_x E/E - \sin\theta\partial_x\theta + \sin\theta\partial_y E/E + \cos\theta\partial_y\theta \\ \cos\theta\partial_y E/E - \sin\theta\partial_y\theta - \sin\theta\partial_x E/E - \cos\theta\partial_x\theta \end{bmatrix}. \tag{20}$$

To recover the sensitivity obtained by the setup of Fig. 2, we take $\theta_i = 0$. In this case, again supposing $\theta_{\mathrm{FR}} \ll 1$, (20) simplifies to

$$\mathbf{E}'(x,y) \simeq E\left[\frac{\partial_x E}{E} + \partial_y\theta_{\mathrm{FR}}\right]\mathbf{x} + E\left[\frac{\partial_y E}{E} - \partial_x\theta_{\mathrm{FR}}\right]\mathbf{y} \tag{21}$$

providing that $\partial_{x,y}\theta_{\mathrm{FR}}/\theta_{\mathrm{FR}} \gg \partial_{x,y}E/E$. This condition is fulfilled when the magnitude of E is excessively large compared to its derivative. Using a polarizing beam splitter, we can record the intensity of the x-polarization given by

$$I'_x(x,y) \simeq \big|E\partial_x E\big[\partial_x E/E + 2\partial_y\theta_{\mathrm{FR}}\big]\big|. \tag{22}$$

We see that the measurement of the FR derivative is now similar to the standard measurement of Section III-A. The bias is $\partial_x E/E$ rather than the "1" seen in (13) and the FR has been replaced by its derivative. So, a high-power beam with small spatial dependence will amplify the FR $\partial_y\theta_{\mathrm{FR}}$ while reducing the inherent bias $\partial_x E/E$. Both will improve the signal-to-noise ratio substantially. Since the intensity of the y-polarization is

$$I'_y(x,y) \simeq \big|E\partial_y E\big[\partial_y E/E - 2\partial_x\theta_{\mathrm{FR}}\big]\big| \tag{23}$$

we can draw a similar conclusion.

IV. Numerical Simulations

In the rest of the article, we use ray tracing [30] with vector Rayleigh–Sommerfeld (VRS) diffraction [31] to compute the effect of each optical element on the intensity and polarization of FR measurements. We used here parameters that can be used to study the magnetic field inside a high-energy-density plasma with similar hardware used in [16] and [17]. The laser beam will span a total of 5 cm with some beam variation that can be controlled by spectral dispersion (e.g., [32]) with a wavelength of 532 nm. The lenses are 2 cm in diameter with a focal length of 25 cm.

A. Quasihomogeneous Beam

We use a laser beam profile in a large region of the ray-tracing domain that is mostly homogeneous and given by

$$E(x,y) = \frac{E_0}{4}\left[1+\tanh\left(x_0 - \frac{|x-x_c|}{\sigma}\right)\right] \times \left[1+\tanh\left(y_0 - \frac{|y-y_c|}{\sigma}\right)\right]$$

where x_c and y_c correspond to the beam center and σ the transition width to 0. With the given parameters the full-width half-maximum is $2x_0$ along the x-axis and $2y_0$ along the y-axis. Due to the effect of boundary conditions, we keep $2x_0$ and $2y_0$ on the order of 75% of the computational domain width along the respective directions. The spatial dependence of E is shown in Figs. 3 and 4. The FR given by

$$\theta_{\mathrm{FR}}(x,y,M) = M\pi\left[\frac{x-x_{\min}}{x_{\max}-x_{\min}} - \frac{1}{2}\right]^2 + M\pi\left[\frac{y-y_{\min}}{y_{\max}-y_{\min}} - \frac{1}{2}\right]^2 \tag{24}$$

where the scaling factor M allows to switch between large and small rotation, $x_{\min}$ and $x_{\max}$ are the domain limits along the

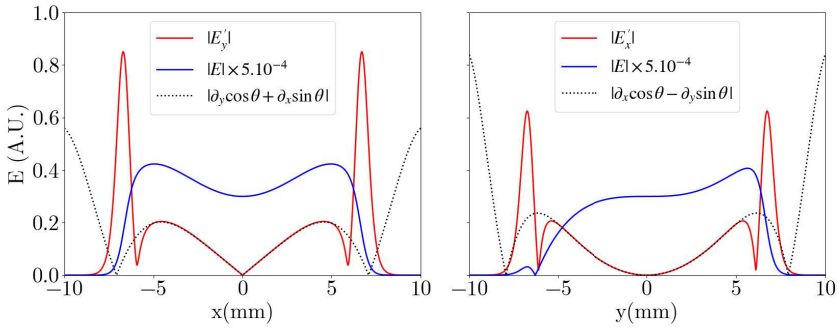

Fig. 3. Electric field of the laser beam downstream of the setup of Fig. 1 along the x-axis for the y-polarization (left) and along the y-axis for the x-polarization (right) for $M = 1$ computed using VRS diffraction. The analytic values of the field are plotted using dotted lines. The magnitude of the initial electric field is indicated in blue.

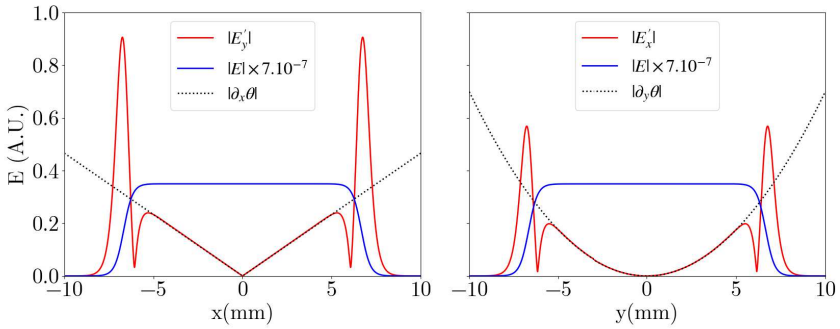

Fig. 4. Electric field of the laser beam downstream of the setup of Fig. 1 along the x-axis for the y-polarization (left) and along the y-axis for the x-polarization (right) computed using VRS diffraction. The analytic values are represented with dotted lines for small rotation angle (i.e., $M = 10^{-3}$), they are approximately $\partial_x\theta_{\mathrm{FR}}$ for the y-polarization (left) and $-\partial_y\theta_{\mathrm{FR}}$ for the x-polarization (right). The magnitude of the initial electric field is indicated in blue.

x-axis, while $y_{\min}$ and $y_{\max}$ are the domain limits along the y-axis. This analytical expression will help to identify the FR feature unequivocally in the downstream beam and verify (9).

For M large (i.e., 1), the downstream electric field should follow (14) and (15), as plotted in Fig. 3. For small rotation angle (i.e., $M = 10^{-3}$), we expect a signal given by (16) and (18). Indeed, we recover the linear dependence of the derivative along the x-axis, shown on the left-hand side of Fig. 4, and the quadratic dependence of the derivative along the y-axis, shown on the right-hand side of Fig. 4.

Here, we scaled the analytical value of the solution given by (14) and (15) to the x-polarization of the output beam profile of Fig. 3 and kept this scaling constant throughout the simulation section.

B. Shaped Beam

As (22) and (23) show, it is possible to recover the sensitivity of the standard method given by (13). However, this can only be achieved if the beam has well-defined spatial variations. In fact, these variations should be as simple as possible to allow for an easy measurement of the rotation. While we are using a laser for getting large intensities allowing us to amplify the rotation signal, the coherence of the beam is not primordial as the S-waveplate affects the phase signal only by adding a constant. As a result, the beam profile can be controlled using engineered diffusers [29] with an extremely high level of precision. We need to use here a diffuser that scrambles the phase rather than the polarization. To this end, we now add a small, linear variation to the previous beam, for example,

$$E(x,y) = \frac{E_0}{4}\left[1+\tanh\left(x_0-\frac{|x-x_c|}{\sigma}\right)\right] \times\left[1+\tanh\left(y_0-\frac{|y-y_c|}{\sigma}\right)\right] \times\left[|\alpha_x x+x_{\mathrm{bias}}|+|\alpha_y y+y_{\mathrm{bias}}|\right] \tag{25}$$

and shown in Fig. 5(a). We also show the impact of the waveplate only [Fig. 5(b)] and the neutral density only in Fig. 5(c). If the variation is too large, then we could be back with a case similar to (13), where the bias decreases the signal-to-noise ratio. However, if this is deemed necessary, we can reduce the impact on the FR signal simply by increasing the base electric field. In this case, the bias terms $\partial_x E/E$ and $\partial_y E/E$ in (22) and (23) can be made small compared to the FR signal, while the amplification terms $E\partial_x E$ and $E\partial_y E$ can be made large, *de facto* amplifying the FR signal. Using the same FR profile of (24), Fig. 6 shows that ray tracing confirms (21). While not plotted, numerical simulations confirm both (17) and (19).

C. Noisy Shaped Beam

It is now time to see what can be done about the beam noise. Clearly, this is an open problem so far, at least for the

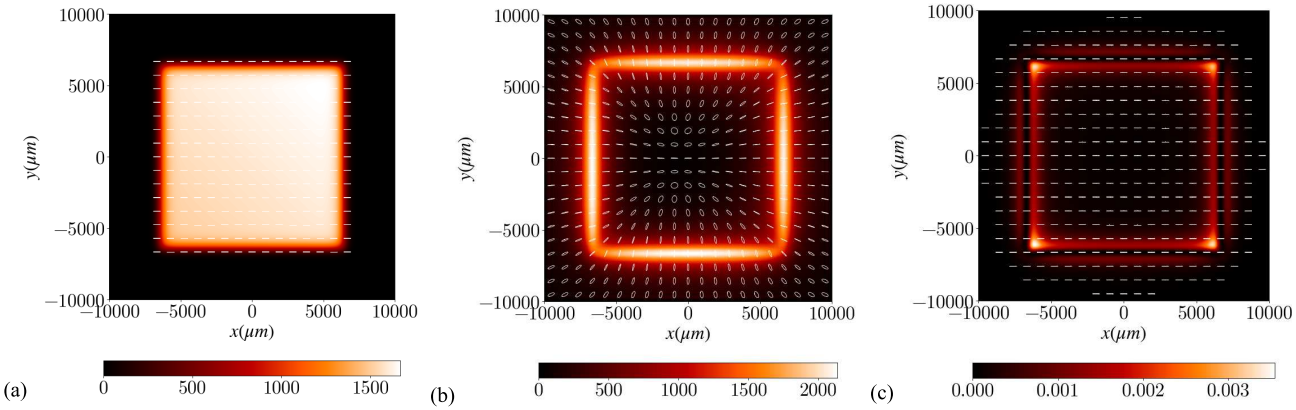

Fig. 5. (a) Shaped beam with polarization given by (25). The shaped beam after the $2-f$ setup using (b) waveplate only and (c) neutral density filter only.

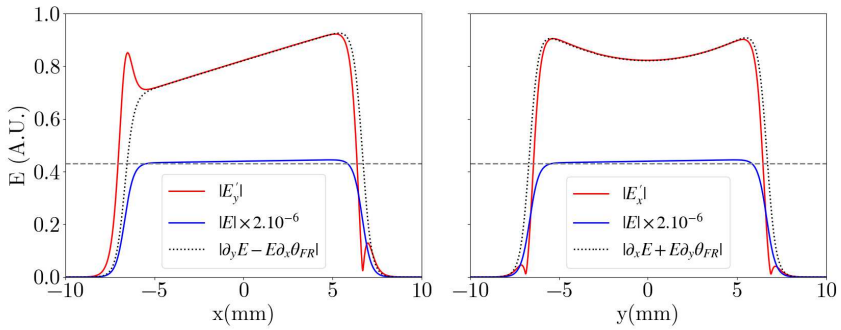

Fig. 6. Electric field of the laser beam downstream of the setup of Fig. 1 along the x-axis for the y-polarization (left) and along the y-axis for the x-polarization (right) computed using VRS diffraction. The analytic values are represented with dotted lines for a small rotation angle (i.e., $M = 10^{-3}$). The initial electric field is indicated in blue. The horizontal dashed line is used to highlight the variation of the electric field of the initial beam.

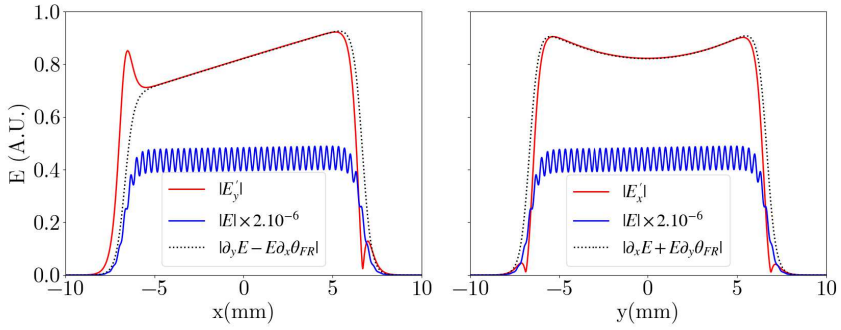

Fig. 7. Electric field of the laser beam downstream of the setup of Fig. 1 along the x-axis for the y-polarization (left) and along the y-axis for the x-polarization (right) using VRS. The expected values are plotted using dotted lines for a small rotation angle (i.e., $M = 10^{-3}$). The initial electric field is indicated in blue and has a noise amplitude of 10%.

low-frequency noise. Yet, several techniques have shown good mitigation. For instance, low-frequency noise can be removed using spectral dispersion [32], [33] or microlens arrays [34], [35]. Polarization smoothing [36] cannot be used here since we are measuring polarization.

High-frequency intensity noise can be removed more easily. This is simply done by placing an aperture in the Fourier plane of the setup shown in Fig. 1 [37]. This can be combined directly inside the neutral density filter of (4), setting the transmission to zero at the filter periphery. Fig. 7 shows that a high-frequency noise up to 10% has almost no impact on the FR measurement, once filtered optically.

V. Conclusion

This work shows that the combination of an S-waveplate with a linearly varying neutral density filter allows to compute the spatial derivative of the FR angle. The y-polarization exiting the setup will carry the partial derivative along the x-axis, while the x-polarization will carry the partial derivative along y. In a standard setup, where the FR signal appears on top of the beam carrier, increasing the beam energy does not necessarily improve the FR signal, except if the background light from the medium (i.e., the continuum) is relatively bright. In this case, larger intensities reduced the impact of the background noise. In the proposed setup, the FR derivative

is proportional to the beam energy. So, the laser acts as an amplifier, allowing to increase the signal simply by increasing the beam energy. In real-life situations, the spatial variation of the beam now adds to the FR signal, as shown by (9). So, it is imperative to smooth the beam to increase the signal-to-noise ratio. One method is simply to expand the beam, possibly beyond the optical system, to reduce unwanted gradients as much as possible near the optical axis. However, high-frequency noise can be removed using spatial filtering, providing that the FR signal varies much more slowly than the beam noise. Further difficulties arise from the high power required to improve the signal-to-noise ratio because of the parasitic plasma light. The high-power laser will be focused directly onto the waveplate and the neutral density filter could get damaged. This problem can be limited by setting the $2-f$ system in a vacuum. It is also possible to move the neutral density filter closer to the first lens. As we move the filter away from the focal point, the light intensity will decrease. Now, because the filter is not located at its optimal position, it will not perform as predicted. However, we can perform a correction on the filter by doing a partial Fourier transform of the filter [38]. Another option is to use a lower-power laser coupled to an intensified ICCD so that the plasma light can be greatly decreased by reducing the exposure time. Furthermore, as the plasma light is broad geometrically, most of the light will be near the focal point in the $2-f$ system. Since the neutral density filter has little transparency for low wavenumbers, we expect an improvement in the signal-to-noise ratio compared to the traditional FR technique.

REFERENCES

[1] J. M. Stone, *Radiation and Optics*. New York, NY, USA: McGraw-Hill, 1963.

[2] L. J. Aplet and J. W. Carson, "A Faraday effect optical isolator," *Appl. Opt.*, vol. 3, no. 4, pp. 544–545, Apr. 1964.

[3] I. B. Zeldovich, A. A. Ruzmaikin, and D. D. Sokolov, *Magnetic Fields in Astrophysics*, vol. 3, 1983.

[4] J. A. Crowther, *The Life and Discoveries of Michael Faraday*. London, U.K.: Society for Promoting Christian Knowledge, 1918.

[5] T. Pisarczyk, A. A. Rupasov, G. S. Sarkisov, and A. S. Shikanov, "Faraday-rotation method for magnetic-field diagnostics in a laser plasma," *J. Sov. Laser Res.*, vol. 11, no. 1, pp. 1–32, 1990.

[6] A. D. Gray, T. L. Landecker, P. E. Dewdney, and A. R. Taylor, "A large-scale, interstellar faraday-rotation feature of unknown origin," *Nature*, vol. 393, no. 6686, pp. 660–662, Jun. 1998.

[7] R. Manchester, "Pulsar rotation and dispersion measures and the galactic magnetic field," *Astrophysical J.*, vol. 172, p. 43, Feb. 1972.

[8] R. Bachiller, "Bipolar molecular outflows from young stars and protostars," *Annu. Rev. Astron. Astrophys.*, vol. 34, no. 1, pp. 111–154, Sep. 1996.

[9] A. Königl, "On the interpretation of the apparent existence of a preferred magnetic polarity in extragalactic jet sources," *Monthly Notices Roy. Astronomical Soc.: Lett.*, vol. 407, no. 1, pp. 79–83, Sep. 2010.

[10] P.-A. Gourdain and C. E. Seyler, "Impact of the Hall effect on high-energy-density plasma jets," *Phys. Rev. Lett.*, vol. 110, no. 1, Jan. 2013, Art. no. 015002.

[11] F. Suzuki-Vidal et al., "Formation of episodic magnetically driven radiatively cooled plasma jets in the laboratory," *Astrophys. Space Sci.*, vol. 322, nos. 1–4, pp. 19–23, Aug. 2009.

[12] P.-A. Gourdain et al., "Initial experiments using radial foils on the cornell beam research accelerator pulsed power generator," *Phys. Plasmas*, vol. 17, no. 1, Jan. 2010, Art. no. 012706.

[13] J. Zhang et al., "Design of a millimeter-wave polarimeter for NSTX-upgrade and initial test on DIII-D," *Rev. Sci. Instrum.*, vol. 83, no. 10, Oct. 2012, Art. no. 10E321.

[14] G. Torrisi, E. Naselli, D. Mascali, L. Di Donato, and G. Sorbello, "Mm-wave polarimeter and profilometry design study for retrieving plasma density in the Pandora experiment," *Frontiers Astron. Space Sci.*, vol. 9, Aug. 2022, Art. no. 949920.

[15] G. F. Swadling et al., "Diagnosing collisions of magnetized, high energy density plasma flows using a combination of collective Thomson scattering, Faraday rotation, and interferometry (invited)," *Rev. Sci. Instrum.*, vol. 85, no. 11, Nov. 2014, Art. no. 11E502.

[16] J. W. D. Halliday et al., "Investigating radiatively driven, magnetized plasmas with a university scale pulsed-power generator," *Phys. Plasmas*, vol. 29, no. 4, Apr. 2022, Art. no. 042107.

[17] V. Valenzuela-Villaseca et al., "Characterization of quasi-keplerian, differentially rotating, free-boundary laboratory plasmas," *Phys. Rev. Lett.*, vol. 130, no. 19, May 2023, Art. no. 195101.

[18] J. Zhang, N. A. Crocker, T. A. Carter, S. Kubota, and W. A. Peebles, "Interaction between Faraday rotation and Cotton–Mouton effects in polarimetry modeling for NSTX," *Rev. Sci. Instrum.*, vol. 81, no. 10, Oct. 2010, Art. no. 10D519.

[19] S. V. Lebedev, A. Frank, and D. D. Ryutov, "Exploring astrophysics-relevant magnetohydrodynamics with pulsed-power laboratory facilities," *Rev. Modern Phys.*, vol. 91, no. 2, Apr. 2019, Art. no. 025002.

[20] M. Beresna, M. Gecevičius, P. G. Kazansky, and T. Gertus, "Radially polarized optical vortex converter created by femtosecond laser nanostructuring of glass," *Appl. Phys. Lett.*, vol. 98, no. 20, May 2011, Art. no. 201101.

[21] T. Bauer, S. Orlov, U. Peschel, P. Banzer, and G. Leuchs, "Nanointerferometric amplitude and phase reconstruction of tightly focused vector beams," *Nature Photon.*, vol. 8, no. 1, pp. 23–27, Jan. 2014.

[22] Q. Zhan, "Cylindrical vector beams: From mathematical concepts to applications," *Adv. Opt. Photon.*, vol. 1, no. 1, pp. 1–57, Jan. 2009.

[23] E. J. Galvez, S. Khadka, W. H. Schubert, and S. Nomoto, "Poincaré-beam patterns produced by nonseparable superpositions of Laguerre–Gauss and polarization modes of light," *Appl. Opt.*, vol. 51, pp. 2925–2934, May 2012.

[24] R. W. Boyd and M. J. Padgett, "Quantum mechanical properties of light fields carrying orbital angular momentum," in *Optics in Our Time*. Cham, Switzerland: Springer, 2016, pp. 435–454.

[25] J. Goodman, *Introduction To Fourier Optics*, 4th ed., New York, NY, USA: W.H. Freeman, May 2017.

[26] P. S. Theocaris and E. E. Gdoutos, *Matrix Theory of Photoelasticity*, vol. 11. Berlin, Germany: Springer, 1979.

[27] F. S. Roux, "Geometric phase lens," *J. Opt. Soc. Amer. A, Opt. Image Sci.*, vol. 23, no. 2, pp. 476–482, 2006.

[28] P.-A. Gourdain et al., "True optical spatial derivatives for direct phase gradient measurements," *Opt. Continuum*, vol. 2, no. 4, pp. 838–846, 2023.

[29] F. M. Dickey, *Laser Beam Shaping: Theory and Techniques*. Boca Raton, FL, USA: CRC Press, 2018.

[30] L. S. Brea, "Diffractio, Python module for diffraction and interference optics," Tech. Rep., 2019.

[31] F. Shen and A. Wang, "Fast-Fourier-transform based numerical integration method for the Rayleigh–Sommerfeld diffraction formula," *Appl. Opt.*, vol. 45, no. 6, pp. 1102–1110, 2006.

[32] S. P. Regan et al., "Experimental investigation of smoothing by spectral dispersion," *J. Opt. Soc. Amer. B, Opt. Phys.*, vol. 17, no. 9, pp. 1483–1489, 2000.

[33] S. Skupsky, R. W. Short, T. Kessler, R. S. Craxton, S. Letzring, and J. M. Soures, "Improved laser-beam uniformity using the angular dispersion of frequency-modulated light," *J. Appl. Phys.*, vol. 66, no. 8, pp. 3456–3462, Oct. 1989.

[34] M. Zimmermann, N. Lindlein, R. Voelkel, and K. J. Weible, "Microlens laser beam homogenizer: From theory to application," *Proc. SPIE*, vol. 6663, Sep. 2007, Art. no. 666302.

[35] J. Meng et al., "Partially coherent beam smoothing using a microlens array," *Opt. Exp.*, vol. 29, no. 26, pp. 44045–44062, 2021.

[36] T. R. Boehly et al., "Reduction of laser imprinting using polarization smoothing on a solid-state fusion laser," *J. Appl. Phys.*, vol. 85, no. 7, pp. 3444–3447, Apr. 1999.

[37] P. Elias, D. S. Grey, and D. Z. Robinson, "Fourier treatment of optical processes," *J. Opt. Soc. Amer.*, vol. 42, pp. 127–134, Feb. 1952.

[38] D. H. Bailey and P. N. Swarztrauber, "The fractional Fourier transform and applications," *SIAM Rev.*, vol. 33, no. 3, pp. 389–404, Sep. 1991.